(This is a sample cover image for this issue. The actual cover is not yet available at this time.)

Earth and Planetary Science Letters 317-318 (2012) 331–342

Contents lists available at SciVerse ScienceDirect

Earth and Planetary Science Letters

journal homepage: www.elsevier.com/locate/epsl

The composition of Earth's oldest iron formations: The Nuvvuagittuq Supracrustal Belt (Québec, Canada)

Aleksandra M. Mloszewska [a,*], Ernesto Pecoits [a], Nicole L. Cates [b], Stephen J. Mojzsis [b,d], Jonathan O'Neil [c], Leslie J. Robbins [a], Kurt O. Konhauser [a]

[a] Department of Earth and Atmospheric Sciences, 1-26 Earth Sciences Building, University of Alberta, Edmonton, Alberta, T6G 2E3, Canada
[b] Department of Geological Sciences, Center for Astrobiology University of Colorado, Boulder, CO, 80309-0399, USA
[c] Department of Terrestrial Magnetism, Carnegie Institution of Washington, Washington DC, 20015-1305, USA
[d] Laboratoire de Géologie de Lyon: Terre, Planètes, Environnement, Université Lyon 1 (Claude Bernard), Ecole Normale Supérieure de Lyon, CNRS UMR 5276, Villeurbanne, France

ARTICLE INFO

Article history:
Received 10 April 2011
Received in revised form 17 October 2011
Accepted 18 November 2011
Available online xxxx

Editor: P. DeMenocal

Keywords:
banded iron formation
Nuvvuagittuq Supracrustal Belt
trace element geochemistry
Eoarchean
Hadean
seawater

ABSTRACT

The composition of iron formations in the ≥3.75 Ga yr old Nuvvuagittuq Supracrustal Belt in northern Québec provides a proxy for seawater composition of the Eoarchean, and perhaps Hadean oceans, as well as constraints on the types of nutrients available to Earth's earliest life forms. Integrated petrologic and geochemical relationships, mapped between mineral phases in thin section and whole-rock chemistry, provide a framework for interpreting bulk and micro-scale variations in these chemical sedimentary precipitates. Results show that there are two distinct chemical sedimentary units in the Nuvvuagittuq belt: i) a banded iron formation (BIF) consisting of alternating micro-bands of magnetite, Ca–Mg–Fe-silicates and quartz, and ii) a more silicate-rich (Fe-poor) unit, the banded silicate-formation (BSF), of alternating micro-bands of quartz and Ca–Mg–Fe silicates. Precursor BIF and BSF deposits were likely layered amorphous silica and ferric-oxyhydroxides, fine-grained carbonate oozes and/or Ca–Mg–Fe rich silicate gels deposited in a marine setting. Low Al_2O_3, TiO_2 and HFSE concentrations show that they are relatively detritus-free, with distinctively seawater-like REE + Y profiles and consistently positive Eu anomalies. These features suggest that the rocks preserved their seawater-like compositions despite metamorphic overprinting. The most significant trace elements in the sediments are Ni and Zn. Experimentally-derived partitioning coefficients show that Ni was enriched in Eoarchean seawater as compared to today (up to 300 nM), while Zn was fairly similar (up to 20 nM). Compositional resemblances between the Nuvvuagittuq sediments and those documented in the ca. 3.8 Ga Isua supracrustals (West Greenland) provide a plausible case that global ocean processes – in terms of trace metal abundances – had reached steady-state by the Eoarchean.

1. Introduction

Banded iron formations (BIF) are iron- and silica-rich marine, chemical sedimentary precipitates that were deposited with some hiatuses throughout the Archean and much of the Proterozoic. Because the precursor minerals of these rocks precipitated directly out of seawater, the primary ferric-oxyhydroxide minerals that comprised the initial sediments retained chemical signatures of the seawater. In this regard, BIF compositions have long been used as proxies for the compositional evolution of seawater over time (e.g. Bau and Dulski, 1996; Bolhar et al., 2004; Jacobsen and Pimentel-Klose, 1988), and ultimately for the types of nutrients that were available to ancient planktonic life (e.g., Bjerrum and Canfield, 2002; Konhauser et al., 2009). For instance, based on documented P:Fe ratios in 3.2 to 1.9 Ga BIF, Bjerrum and Canfield (2002) proposed that the Archean–Paleoproterozoic oceans may have been phosphate limited. This condition could have hindered initial cyanobacterial phytoplanktonic growth, and consequently delayed the rise of oxygen until the demise of Fe(II)-rich marine waters that accompanied the decline of BIF deposition in the Paleoproterozoic. Konhauser et al. (2009) used Ni/Fe ratios to infer a trace metal crisis starting at around 2.7 Ga for methanogenic bacteria, and proposed that the subsequent decline of methanogens aided in the rise of atmospheric oxygen. It is noteworthy that the metabolic trace metal requirements of ancient microbes could have been established by their bioavailability in the ancient oceans, and that a record of this is preserved in the genomes of their modern descendants (daSilva and Williams, 1991; Saito et al., 2003).

Although banded iron formations formed throughout much of the Precambrian, the paucity of pre-3.5 Ga supracrustal rocks severely hampers the use of BIFs for discerning compositional changes in Earth's earliest oceans and hence of the nature of habitats for putative early life forms. By far the most intensely studied Eoarchean BIFs are

* Corresponding author. Tel.: +1 11 780 250 1201; fax: +1 11 780 492 2030.
E-mail address: mloszews@ualberta.ca (A.M. Mloszewska).

0012-821X/$ – see front matter © 2011 Elsevier B.V. All rights reserved.
doi:10.1016/j.epsl.2011.11.020

from the Isua Supracrustal Belt (ISB), as well as various BIF enclaves (termed the Akilia association) scattered throughout the ca. 3000 km^2 Itsaq Gneiss Complex in West Greenland (Nutman et al., 1996). Much of the published work from these complex BIFs has focused on describing (and debating) their origins (e.g., Cates and Mojzsis, 2006; Dauphas et al., 2004; Dauphas et al., 2007b; Dymek and Klein, 1988; Frei and Polat, 2007; Manning et al., 2006; Polat and Frei, 2005; Whitehouse and Fedo, 2007). The recent discovery of well-preserved, banded quartz–magnetite units of BIF protolith, and another composed of banded quartz and Fe-silicate minerals (hereafter termed BSF), in the Nuvvuagittuq Supracrustal Belt in Northern Québec provides an excellent opportunity to study the early oceans especially in the context of global environmental conditions which led to BIF sedimentation. The belt is at least 3.75 Ga in age, and perhaps as old as 4.28 Ga (cf. Cates and Mojzsis, 2007, 2009; O'Neil et al. 2008, 2011 — see Section 2).

While research on the Nuvvuagittuq rocks is still in its infancy, preliminary chemical and isotopic work has conclusively shown that the BIF, and a representative portion of the BSF, possess many distinguishing characteristics of rocks of chemical sedimentary protolith (Cates and Mojzsis, 2007; Dauphas et al., 2007a, 2007b; O'Neil et al., 2007). Bulk chemical analyses further indicate that these rocks retain seawater-like rare earth element and yttrium (REE + Y) signatures such as concave-upward profiles, positive La and Eu anomalies and superchondritic Y/Ho ratios (Bolhar et al. 2004; Cates and Mojzsis, 2007; Dauphas et al. 2007a; O'Neil et al., 2007).

A currently acknowledged possibility for the origins of the Fe-oxide layers in BIF is that they were a by-product of microbial metabolism (Konhauser et al., 2002). Dauphas et al. (2007a) pointed out that the relatively heavy Fe-isotope compositions of Nuvvuagittuq ferruginous quartz–amphibole rocks of chemical sedimentary protolith can be most simply explained by a microbial oxygenic or anoxygenic photosynthetic origin. If correct, this underscores the notion that microbial life was already established at the beginning of the sedimentary rock record. Hence, any reliable means to estimate concentrations of solutes in pre-3.5 Ga seawater would reveal new insights into the nutrient status of the oceans from which key microbial metallo-enzymes first evolved. BIF compositions also potentially provide a measure of the balance that both mantle and surface processes had on seawater composition through time (e.g. Isley, 1995), and it is well established that seawater composition as reflected in BIF is influenced by both hydrothermal, and in many cases, terrestrial inputs (Bau, 1993; Bolhar et al. 2004; Hamade et al., 2003).

In this study, we performed detailed geochemical mapping of candidate Nuvvuagittuq chemical sediments (BIF, BSF) that integrated the petrologic and geochemical relationships between mineral phases in thin section and whole-rock chemistry to provide a framework for interpreting their bulk and microscale variations. These data were used to construct a model of seawater compositions in the Nuvvuagittuq basin as a first-order constraint on the geochemical evolution of seawater on the post-bombardment Earth.

2. Geological setting

The geology of the Nuvvuagittuq belt and surrounding gneisses has been reviewed elsewhere (Boily et al., 2009; Cates and Mojzsis, 2007, 2009; David et al., 2009; O'Neil et al., 2007; Stevenson et al., 2006), and hence, only a brief synopsis is provided here. Tonalite gneisses immediately surrounding the belt are dated at ca. 3.66 Ga (David et al. 2009). Zircons recovered from trondhjemitic gneisses within the mostly mafic Nuvvuagittuq succession provide ^{207}Pb/^{206}Pb ages of 3751 ± 10 Ma (Cates and Mojzsis, 2007), and a similar age of 3817 ± 16 Ma was obtained from zircons from the same unit (David et al., 2009), which establishes that the belt is at least Eoarchean in age. Also, intruding gabbros give a ^{147}Sm–^{143}Nd isochron age of 4023 ± 110 Ma, while a cummingtonite-rich amphibolites provide a ^{142}Nd/^{144}Nd vs. ^{147}Sm/^{144}Nd isochron age of $4280 \pm {}^{53}_{81}$ Ma (O'Neil et al., 2008).

Subsequent to re-working in the Eo- and Mesoarchean, the terrane was intruded by Neoarchean, εNd depleted TTG (tonalite–trondhjemit–granodiorite) and GGM (granite–granodiorite–monazite) suites (where the εNd notation defines the departure of ^{143}Nd/^{144}Nd from the Chondrite Uniform Reservoir evolution line), as well as by mafic to felsic volcanic suites with enriched εNd signatures thought to have been derived from the recycling of Mesoarchean crust (Boily et al., 2009). The Nuvvuagittuq belt is an isoclinal, north-plunging synform that has been refolded into a more open, south-plunging synform (Fig. 1; David et al., 2009; O'Neil et al., 2007, 2011). It has undergone extensive retrograde metamorphism from upper amphibolite/lower granulite facies to greenschist facies, and thermobarometry experiments by Cates and Mojzsis (2009) suggest that metamorphic temperatures were as high as ~640 °C. At least three major metamorphic events are recorded through U–Pb zircon dating methods at ca. 3.6 Ga, 3.3 Ga and 2.7 Ga; the latest event is thought to be related to the juxtaposition of the Hudson Bay and Arnaud River terranes (Cates and Mojzsis, 2009; David et al., 2009).

In the broadest of terms, the Nuvvuagittuq belt can be divided up into three main units: (1) a cummingtonite-rich amphibolite previously referred to as the "faux-amphibolite" (O'Neil et al., 2007, 2008) because of its lack of hornblende as in more common amphibolitized basalts, and now referred to as the Ujaraaluk unit by O'Neil et al. (2011); (2) gabbroic and ultramafic conformable bodies interpreted by O'Neil et al. (2008, 2011), as sills (cf. Cates and Mojzsis, 2007); and (3) rocks of likely chemical sedimentary protolith, including banded iron formation (Fig. 1). The amphibolite unit is the most voluminous of the three main rock types. It has a generally basaltic to andesitic composition and locally preserves millimeter- to meter-scale compositional layering, and has been interpreted to be an altered mafic volcanic pyroclastic deposit (O'Neil et al., 2011). The progression from chlorite–epidote-bearing rocks and garnet-free cummingtonite amphibolites in the western portion of the belt, to garnet-bearing cummingtonite amphibolites in the east suggests a map-scale metamorphic gradient from upper-greenschist-facies in the west to upper-amphibolite facies in the east (O'Neil et al., 2007).

The amphibolite unit can be divided into three stratigraphically superimposed, geochemically distinct groups (O'Neil et al., 2011) with the iron formation units positioned between two of these groups. The group stratigraphically below these units has high Ti content, low Al/Ti ratios and relatively flat REE profiles, whereas the two groups above are characterized by low Ti contents and higher Al/Ti ratios. The group directly above has the highest Al/Ti ratios and displays distinct U-shape REE profiles with low Ta and Nb. The group at top of the sequence also has large negative Ta and Nb anomalies, but is characterized by enriched LREE profiles. The transition between low Al/high Ti amphibolites to the high Al/low Ti amphibolites is interpreted by O'Neil et al. (2011) to represent a transition from rocks resembling those of oceanic tholeiites to rocks sharing chemical features typically observed in a volcanic island arc setting. Regardless of tectonic setting, the iron formation units occur stratigraphically at the transition between the geochemically distinct amphibolites.

The 5–30 meter wide BIF is composed of alternating bands of magnetite and grunerite with variable amounts of, locally, finely layered quartz (0.1–0.3 cm), which outcrops continuously along the western limb of the synform and discontinuously along the eastern limb (Fig. 1). Positioned ~50 m up section from this unit is a fine- to coarsely-banded unit (0.1–1 cm) of alternating Fe–Ca–Mg silicate (grunerite, actinolite and pyroxene) and quartz bands (Fig. 1). It can be traced continuously down the western limb of the fold and discontinuously around to the southern tip of the belt. This unit grades

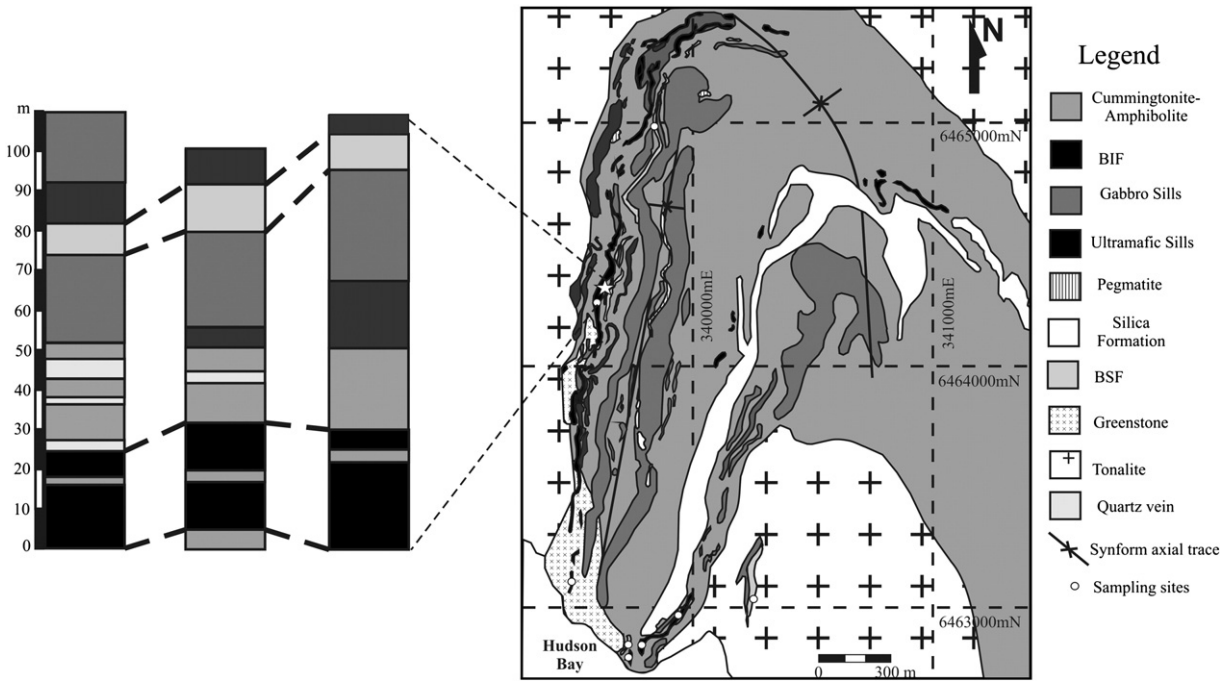

Fig. 1. Map of the Nuvvuagittuq Supracrustal Belt (Northern Québec) showing the main rock units and sampling sites, and the stratigraphy of the chemical sediments on the western side of the belt (O'Neil et al. 2007, 2011).

into a 100 m-wide cherty unit composed of recrystallized quartz with minor amounts of disseminated pyrite, on the western limb of the fold (O'Neil et al., 2007). The repetitive sequence of these units on either limb of the fold suggests that some of the original volcano-sedimentary succession of the belt has been preserved despite numerous post-depositional disturbances.

3. Methods

Polished thin sections of samples were prepared and used for reflected and transmitted light microscopy in order to establish the mineralogy and petrology. Nine representative samples of the BIF and BSF were selected for bulk trace element analysis; rocks were broken and sub-sampled to avoid secondary veining and strongly recrystallized areas. Samples were crushed in a tungsten-carbide mill and the rock powder submitted for bulk XRF and ICP-MS analysis on a PerkinElmer Elan6000 quadrupole inductively coupled plasma mass spectrometer (Quad-ICP-MS) at the University of Alberta (Edmonton, Canada). Mineral-phase chemistry of major (K, Na, Si, Fe, P, Mg, Al, Mn) elements was determined and backscattered-electron images as well as elemental maps produced on the University of Alberta's JEOL 900 electron microprobe. Analytical conditions used on the electron microprobe were: beam diameter (3 μm); voltage (20 kV); current (20 nA); and concentrations were calculated using ZAF matrix correction. Mineral-phase trace element chemistry was analyzed using a Quad-ICP-MS coupled to a laser ablation system with the following analytical conditions: PR power (1200 W); peak hopping acquisition (50 ms dwell time); spot diameter (between 60 μm and 100 μm depending on grain size); repetition rate (5 Hz); and energy density (~13 J/cm^2). The international glass standard NIST SRM 610 was used to calibrate the instrument and Fe concentrations from the electron microprobe were used as an internal standard for each analysis. GLITTER© (XP version, New Wave Research) software was used for data reduction. Bulk XRF analyses were carried out at Activation Laboratories Ltd. (Ancaster, Ontario).

4. Results

4.1. Petrography and mineral chemistry

Rocks of chemical sedimentary protolith in the Nuvvuagittuq belt preserve an upper amphibolite (locally to lower granulite facies) metamorphic assemblages, are coarsely crystalline and are well-banded where silica mobility did not result in complete recrystallization. The BSF consists of fine to coarse (>0.1 mm-wide) bands of quartz which alternate with bands consisting of grunerite [$(Fe,Mg)_7(Si,Al)_8O_{22}$], augite [$Ca(Fe,Mg)(Si,Al)_2O_6$], and actinolite[$(Ca,Na,Mn)_2(Fe,Mg)_5(Si,Al)_8O_{22}$] (Fig. 2A). Actinolite, which was only observed in the BSF, typically occurs as lamellae within a grunerite host. Magnetite (Fe_3O_4) is scattered throughout these Fe-bearing silicate layers, while calcite, pyrite and anorthite (in one sample only, 090709–3) occur as accessory phases (together making up <2 modal % of the rock). The BIF ranges from fine (<300 μm to 0.3 cm-thick) alternating bands of quartz, magnetite and grunerite (<70 μm-wide), to the more common assemblage of fine, alternating bands of grunerite and magnetite with quartz and augite scattered throughout (Fig. 2B,C). The occurrence of pyroxene in these samples corroborates with observations in previously published work on the Nuvvuagittuq chemical sediments (Cates and Mojzsis, 2007; Dauphas et al., 2007a; David et al., 2009). A summary of mineral geochemical analyses are presented in Table 1, and full analyses are available in the Supplementary Data.

4.1.1. Magnetite

Magnetite is the main Fe-oxide mineral component of the Nuvvuagittuq chemical sediments, occurring as a dominant constituent of the BIF (<40 modal %) and as a minor constituent of the BSF (<10 modal %). In both units, magnetite occurs as anhedral to subhedral grains typically between 50 and 200 μm in size. Magnetite in the BSF occurs as individual grains typically associated with the grunerite, and are found both in grain-boundary contact with and as inclusions in grains of grunerite, quartz and augite (Fig. 2A,D). In contrast, magnetite in the BIF comprises defined Fe-oxide bands that range in size from 250 μm to

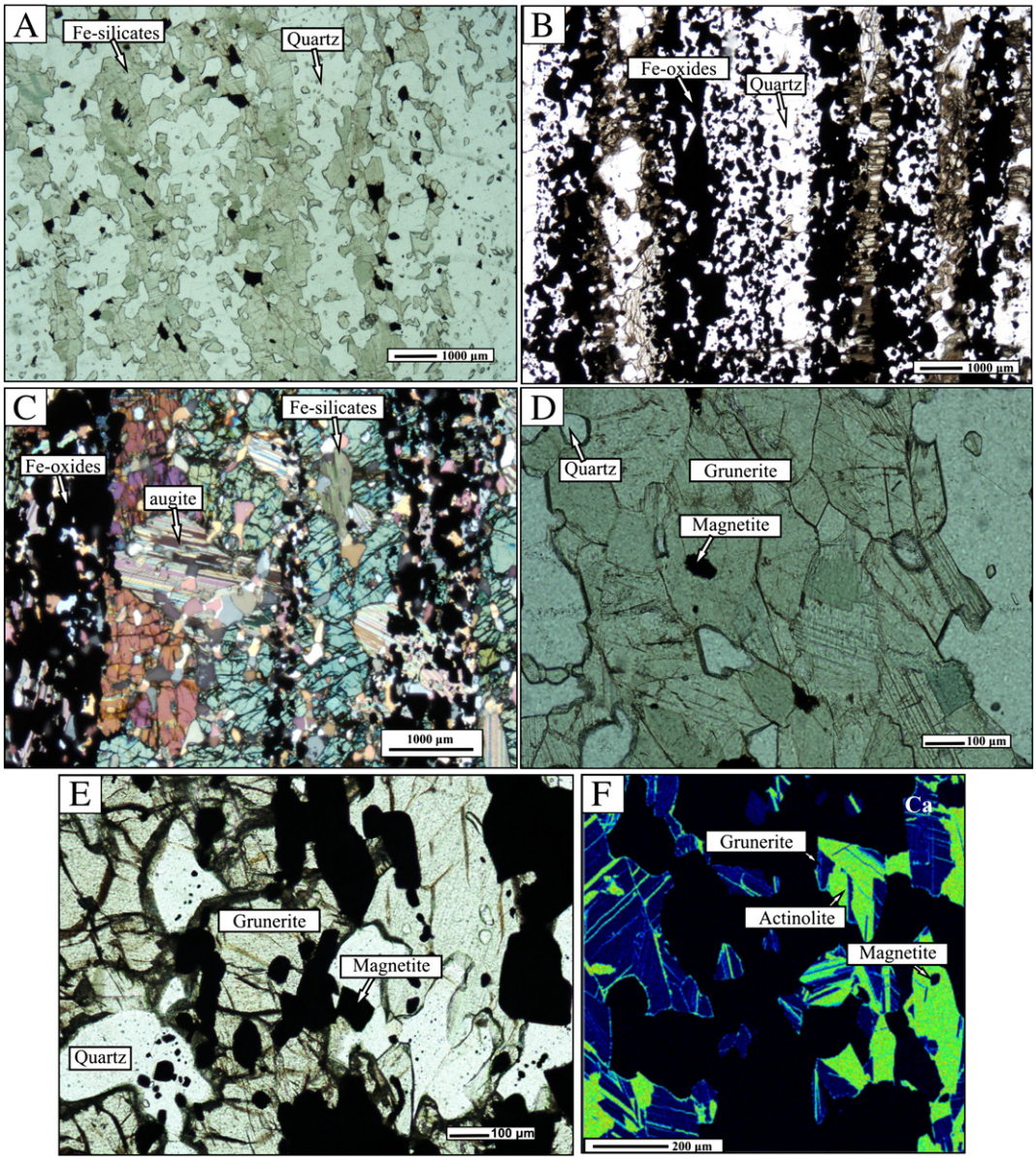

Fig. 2. Photomicrographs and EMP maps showing representative textures and petrographic relationships between the main mineral phases in the BSF (090710–13) and BIF (090709-4b; 090709–5) units. (A) BSF consisting of alternating Fe-silicate (grunerite, actinolite, augite) and quartz bands, and magnetite (black grains) associated with Fe-silicate bands (scale: 1000 µm). (B) BIF consisting of alternating Fe-oxide (magnetite), Fe-silicate (grunerite, augite) and quartz bands (scale: 1000 µm). (C) BIF consisting of alternating Fe-oxide and Fe-silicate bands; quartz and augite are associated with both types of bands (scale is 1000 µm). (D) Fe-silicate band in a BSF showing mineral grains relationships between magnetite, quartz and grunerite (scale: 100 µm). (E) A magnetite and Fe-silicate band in a BIF showing mineral phase relationships between quartz, magnetite and grunerite grains (scale: 100 µm). (F) EMP map (Ca) of an Fe-silicate band in BSF showing lamellae of actinolite hosted by grunerite (scale: 200 µm).

0.3 cm thick, occurring both as individual grains and as large aggregates. Smaller individual magnetite grains are typically found as inclusions within grains of grunerite, quartz and clinopyroxene (Fig. 2E).

Chemical analyses of magnetite in both BIF and BSF show that they are overwhelmingly iron-rich (FeO_{total} 93–94 wt.%) with BIF magnetite slightly more Al_2O_3 and SiO_2-rich (~0.5 and 0.2 wt.% vs. <0.1 wt.%). In BSF magnetite, Cr, Ni and V occur in the highest concentrations of all the trace elements while in BIF magnetite Ni and Zn occur in the highest concentrations, and average concentrations of all other trace elements are below 35 ppm. For most trace metals BIF magnetite is also enriched compared to BSF magnetite (Table 1, Fig. 3A,B).

4.1.2. Quartz

Quartz makes up to 60 modal% of the BSF and 20–60 modal% of the BIF (Fig. 2A–C). Quartz in the BSF occurs as bands and as individual grains within grunerite bands, and is often found as inclusions within grains of grunerite and clinopyroxene. Much of the quartz has a granoblastic-texture, suggestive of static recrystallization. In some BSF samples the quartz is large and has an anhedral habit, extending to over 0.5 cm in size. This larger quartz component shows signs of deformation such as the presence of subgrains, undulose extinction and sutured grain margins. In most of the BIF samples, quartz occurs as individual, 50 to 300 µm-large anhedral to euhedral grains as well as granoblastic-textured aggregates within the grunerite and magnetite bands; aggregates commonly grade into individual grains along a particular band, and some aggregates cross-cut the banding. In one BIF sample (090709–5), quartz makes up regular, 0.5 mm to 2 mm wide, granoblastic-textured bands alternating with the magnetite bands.

Major element composition for quartz is ~100 wt.% SiO_2. The average trace element composition of BSF quartz is below 35 ppm. In BIF

Table 1
Summary of geochemical analyses of selected minerals. <D.L is below detection limit. Reported data are median values. See Supplementary Data for full analyses.

wt.%	Magnetite		Quartz		Grunerite		Augite		Actinolite
	BIF	BSF	BIF	BSF	BIF	BSF	BIF	BSF	BSF
SiO_2	0.16	0.06	101.23	99.59	49.04	52.38	50.47	51.37	52.73
Al_2O_3	0.46	0.01	0.03	0.01	0.14	0.22	0.11	0.28	1.52
TiO_2	0.02	0.01	0.00	0.00	0.04	0.02	0.02	0.00	0.03
FeO_{total}	92.73	93.93	0.36	0.01	46.79	30.17	21.46	11.92	18.70
MgO	0.02	0.01	0.01	0.01	4.97	12.72	6.73	10.76	12.51
MnO	0.02	0.08	<D.L	<D.L	0.48	0.99	0.23	0.96	0.43
CaO	0.00	0.03	<D.L	<D.L	0.63	0.85	21.44	23.33	11.58
K_2O	0.00	0.00	0.00	0.00	0.01	0.11	0.00	0.00	0.02
P_2O_5	0.00	0.01	0.00	0.00	0.05	0.05	0.00	0.00	0.01
ppm									
Sc	2.35	<D.L	3.64	3.97	3.72	1.78	30.66	55.42	37.57
V	6.50	51.56	5.16	1.55	1.46	7.23	1.34	78.77	36.34
Cr	25.67	68.78	13.27	8.09	5.78	7.09	10.92	699.69	47.33
Ni	93.61	54.58	36.01	13.25	45.48	81.56	49.79	157.58	66.10
Co	11.27	1.80	11.05	2.72	15.70	32.04	9.57	51.41	26.35
Cu	1.62	0.76	5.18	3.32	1.40	1.33	1.57	8.15	1.46
Zn	63.63	25.58	86.61	15.27	157.08	166.09	88.61	210.11	197.91
Ga	4.08	13.93	1.18	0.51	0.80	1.38	0.93	3.09	4.85
Ge	22.39	6.52	11.87	1.62	16.16	5.58	20.69	7.52	7.85
Rb	0.32	0.31	1.32	1.74	1.69	3.85	0.49	<D.L	<D.L
Sr	0.29	0.34	0.57	0.34	0.58	0.50	57.76	7.95	11.43
Y	0.39	0.54	4.77	1.08	8.26	11.49	81.28	5.70	38.24
Zr	0.43	0.81	0.48	0.52	0.27	0.60	2.88	2.47	2.55
Nb	0.36	0.67	0.33	0.18	0.19	0.27	0.95	0.40	1.16
Mo	2.31	0.51	1.42	0.17	0.25	0.26	0.49	0.61	0.66
Cd	1.57	0.60	0.21	1.19	0.34	0.35	0.61	1.61	1.61
Hf	0.32	0.49	0.12	0.16	0.09	0.07	0.54	0.33	0.19
Ta	0.22	0.31	0.10	0.12	0.03	0.03	0.21	<D.L	0.21
Pb	0.51	0.33	1.64	0.37	0.21	0.01	0.78	3.54	0.44
Th	0.16	0.14	0.62	0.04	0.08	0.29	0.22	0.08	0.20
U	0.11	<D.L	0.16	0.07	0.05	0.03	0.04	0.07	0.05

quartz, only Zn occurs at concentrations >36 ppm. Similar to the magnetite, BIF quartz is higher in most trace elements than the BSF quartz (Table 1; Fig. 3C,D).

4.1.3. Grunerite

Grunerite in the BSF is composed of <0.3 cm-wide bands that alternate with quartz bands, and occurs as anhedral to subhedral grains. Grunerite grains are hosts to lamellae of actinolite, a feature not observed in the BIF (Fig. 2F). In the BIF, grunerite tends to be noticeably larger in size, varying from 50 μm to at least 2 cm in length, often making up the whole grunerite band along the length of the thin section. Magnetite, quartz and augite grains can be found as inclusions within the grunerite (Fig. 2C,E). In BIF sample 090709–5, bands of magnetite and quartz alternate with thin (<70 μm-wide) bands of grunerite, however the inconsistent distribution of these bands between the magnetite and quartz banding might suggest that this is a primary texture (Fig. 2B).

Major element analyses for grunerite show SiO_2 of 50–52 wt.%. BIF grunerite has higher average FeO_{total} than BSF grunerite (47 wt.% compared to 30 wt.%), while average MgO is lower in the BIF grunerite (5 wt.% compared to 13 wt.%). Of all the trace elements, grunerite has the highest Zn and Ni concentrations while all other trace elements have concentrations below 35 ppm. In contrast to magnetite and quartz, BSF grunerite has higher average trace element concentrations than BIF grunerite (Table 1; Fig. 3E,F).

4.1.4. Augite

Augite in the BSF is associated with the grunerite bands, while in the BIF, it is associated with both grunerite and magnetite bands. In both units, it occurs as individual, 20 to 150 μm large, anhedral to subhedral grains, commonly with inclusions of quartz and magnetite, and can also be found as an inclusion in grunerite (Fig. 2C). Within a single crystal, bands of different interference colors under polarized light points to compositional zoning; exsolved lamellae of orthopyroxene are reportedly common in calcic clinopyroxenes (Deer et al., 1992).

Major element analyses for augite show SiO_2 around 51 wt.% and CaO between 21 and 23 wt.%. FeO_{total} for BIF augite if higher than for BSF augite (21 wt.% compared to 12 wt.%), while MgO is slightly lower in the BIF augite (7 wt.% compared to 11 wt.%). Trace element analyses show that BSF augite is significantly more enriched in Sc, V, Ni, Co and Zn than in the BIF augite where Sr and Y occur in higher concentrations (Table 1; Fig. 3G,H). The augite in sample 090709–3 is especially high in Cr compared to augite in the other BSF samples (500 ppm compared to below detection limit).

4.1.5. Actinolite

Actinolite was only observed in the BSF, but is also mentioned in previous publications on the Nuvvuagittuq chemical sediments as a minor component of the BIF unit (e.g. O'Neil et al., 2007). Actinolite is associated with the grunerite bands of the BSF, and occurs most commonly as lamellae within a grunerite host. They can also be found as anhedral to subhedral, >50 μm-large grains (Fig. 2F).

Major element analyses of actinolite show average compositions of SiO_2 at ~53 wt.%; FeO_{total} at ~20 wt.%; CaO at ~13 wt.%, and MgO at 12 wt.%. In terms of the trace elements, actinolite contains high Zn (198 ppm), Ni (66 ppm) and Cr (47 ppm,) while the average composition of most other trace elements is below 37 ppm (Fig. 3I).

4.2. BSF bulk geochemistry

The BSF is characterized by high, but variable, concentrations of SiO_2 (28–90 wt.%), $Fe_2O_{3\ total}$ (2–55 wt.%), MgO (2–12 wt.%) and CaO (3–16 wt.%) while all other oxides occur in concentrations below 2 wt.% (Fig. 4A, Supplementary Data). The concentrations tend to vary from sample to sample depending on the relative percentage of each mineral phase; sample 090709–3 has the highest Si, Al, and Ti concentrations and the lowest Fe concentrations. Ni, Cu

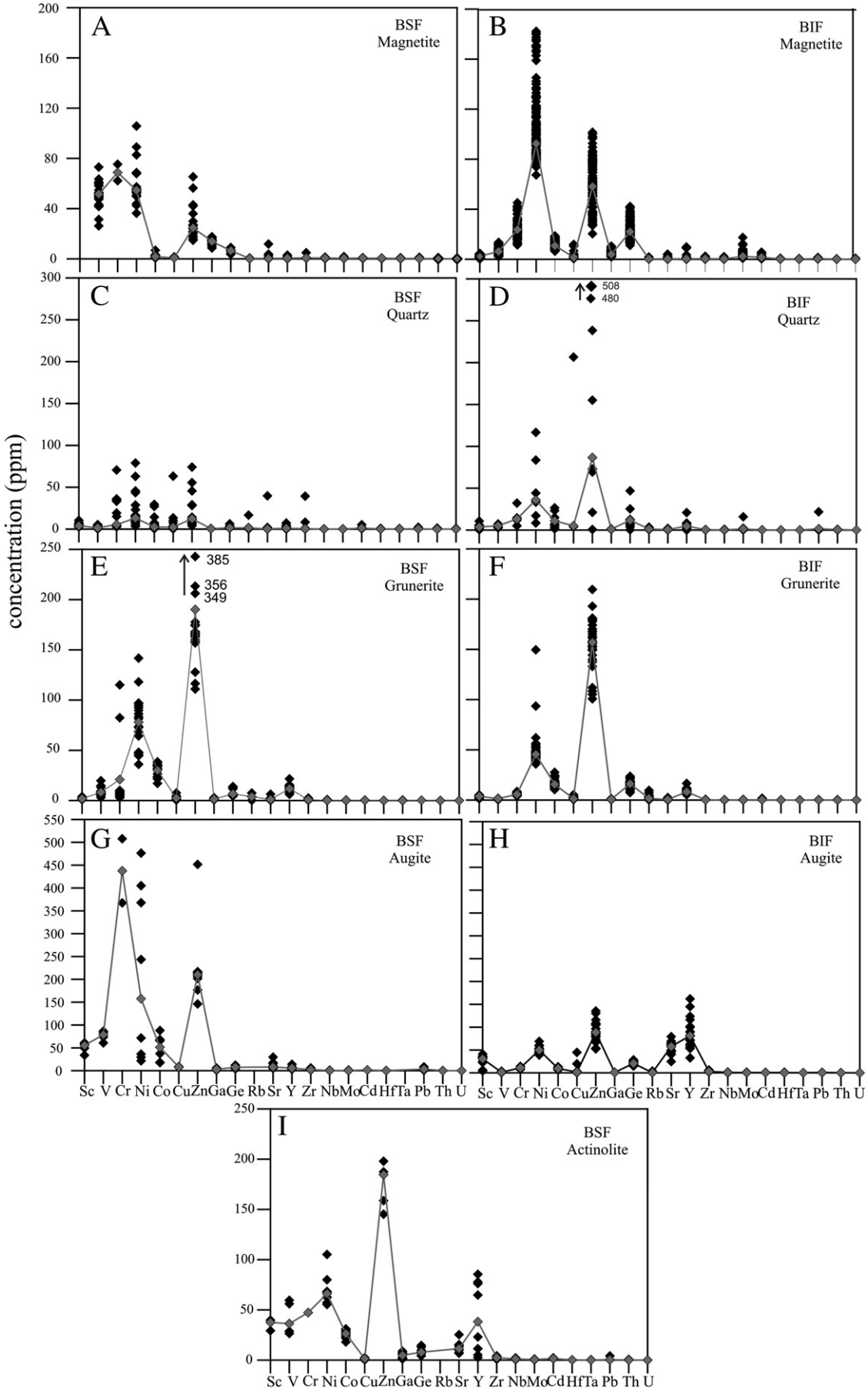

Fig. 3. Plots showing selected trace element chemistry of the main mineral phases (magnetite, quartz, grunerite, augite and actinolite) in the BSF units on the right, and BIF units on the left.

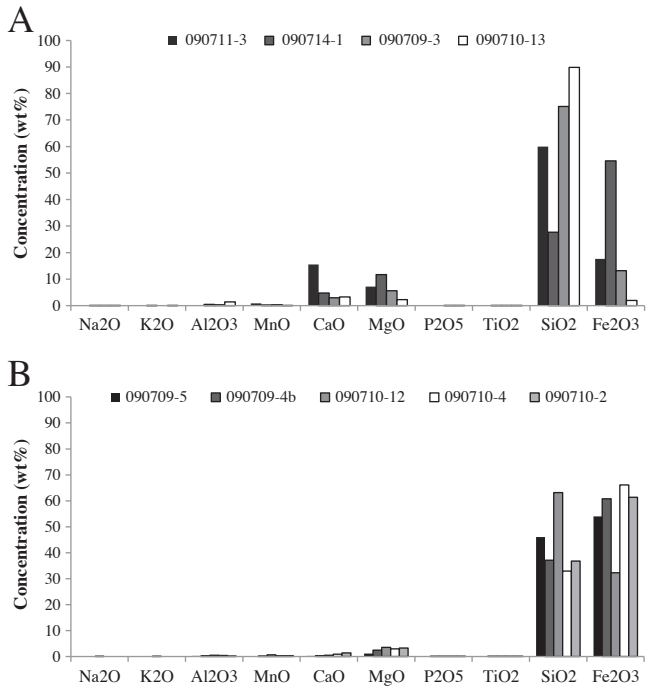

Fig. 4. Plots showing the bulk composition of the major elements in (A) the BSF and (B) the BIF.

and Zn vary greatly from sample to sample, sometimes by up to three orders of magnitude (Fig. 5A). All the BSF samples are highest in Ni and Zn compared to the other trace elements. Sample 090710–13 is significantly higher in Cu and S compared to the other samples suggesting the presence of sulfide grains, and has the highest concentrations of incompatible elements. The other samples have concentrations of Hf and Th <0.5 ppm, Zr <3 ppm, and Y <5 ppm. The

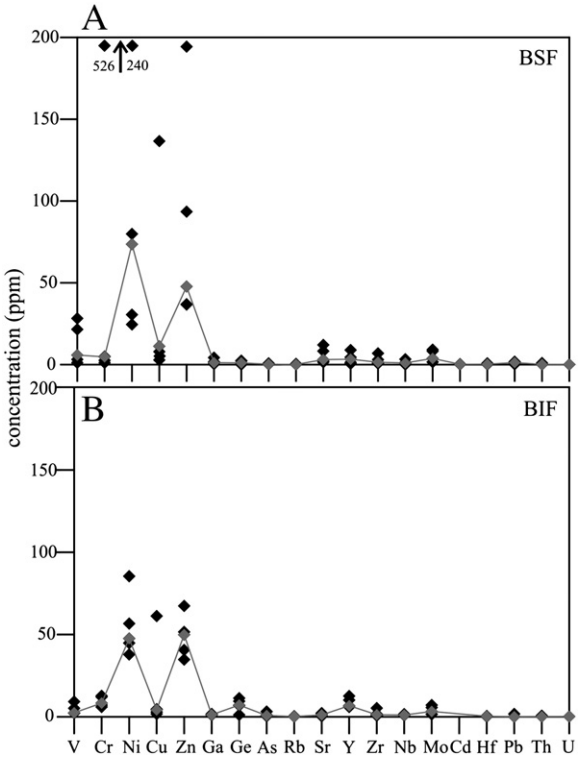

Fig. 5. Bulk major element composition of (A) BSF and (B) BIF. Median values are represented by the gray line.

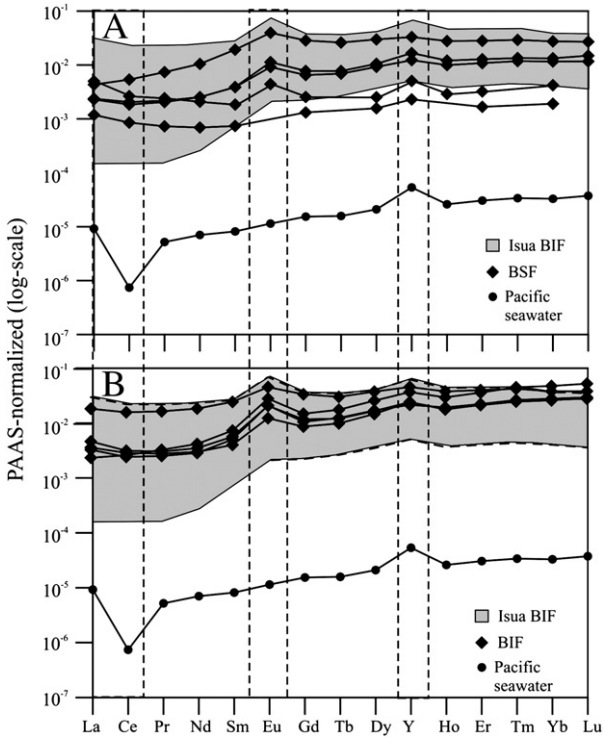

Fig. 6. Shale-normalized bulk REE + Y profiles for (A) BSF and (B) BIF, with REE + Y profile of Pacific seawater (Alibo and Nozaki, 1999) for comparison, and range of REE + Y profiles for Isua BIF (Bolhar et al., 2004). Sample 090710–13 (BSF) has the highest REE + Y abundances of all the BSF samples and flattest profile, whereas sample 090710–12 (BIF) has the highest REE + Y concentrations and flattest profile of the BIF samples.

remainder of the trace elements generally have concentrations <35 ppm. Bulk Post Archean Average Shale composite (PAAS — Taylor and McLennan, 1985) normalized REE + Y profiles for the BSF show; (i) positive La/La* anomalies (2.31 ± 1) (Fig. 7A); (ii) strong positive Eu/Eu* anomalies (1.84 ± 0.16) (Fig. 7B); (iii) superchondritic Y/Ho ratios (37.40 ± 6.83); (iv) depleted LREE relative to HREE (Pr/Yb_{sn}: 0.30 ± 0.19), and (v) MREE relative to HREE (La_{sn}/Yb_{sn}: 0.70 ± 0.23). With the exception to Eu and Ce anomalies, the overall REE + Y profile is similar to that of modern-day seawater (Fig. 6A; e.g., Bolhar et al., 2004). Sample 090710–13 has the highest REE + Y concentrations of all the samples and the flattest overall profile.

4.3. BIF bulk geochemistry

The BIF is characterized by high, variable concentrations of SiO_2 (33–63 wt.%) and Fe_2O_{3total} (32–66 wt.%), while the other major element oxides occur in concentrations <3 wt.% (Fig. 4B, Supplementary Data). Only P is slightly higher in the BIF (0.01–0.09 wt.%) when compared to the BSF. Sample 090710–12 has the highest SiO_2 and lowest Fe_2O_3 concentrations of all the BSF samples; the simultaneously high Cu and S concentrations suggest a contribution by sulfide minerals to the composition of this sample (Supplementary Data). Similar to the BSF, Ni and Zn have the highest concentrations for transition metals in the BIF, while all others are <15 ppm (Fig. 5B). In terms of incompatible elements, Hf and Th have average concentrations of 0.3 ppm; Zr has slightly higher average concentrations of 2 ppm, while Y is even higher at 9 ppm. The shale-normalized REE + Y profile is characterized by; (i) positive La/La* anomalies (1.73 ± 0.34) (Fig. 7A); (ii) strong positive Eu/Eu* anomalies (2.21 ± 0.44) (Fig. 7B); (iii) superchondritic Y/Ho ratios (33.82 ± 2) (Fig. 7C); and (iv) depleted LREE relative to HREE (Pr/Yb_{sn}: 0.16 ± 0.17) and MREE relative to HREE (La_{sn}/Yb_{sn}: 0.47 ± 0.27). The overall REE + Y profiles, which resemble ones from BIF analyzed by O'Neil et al. (2007), are

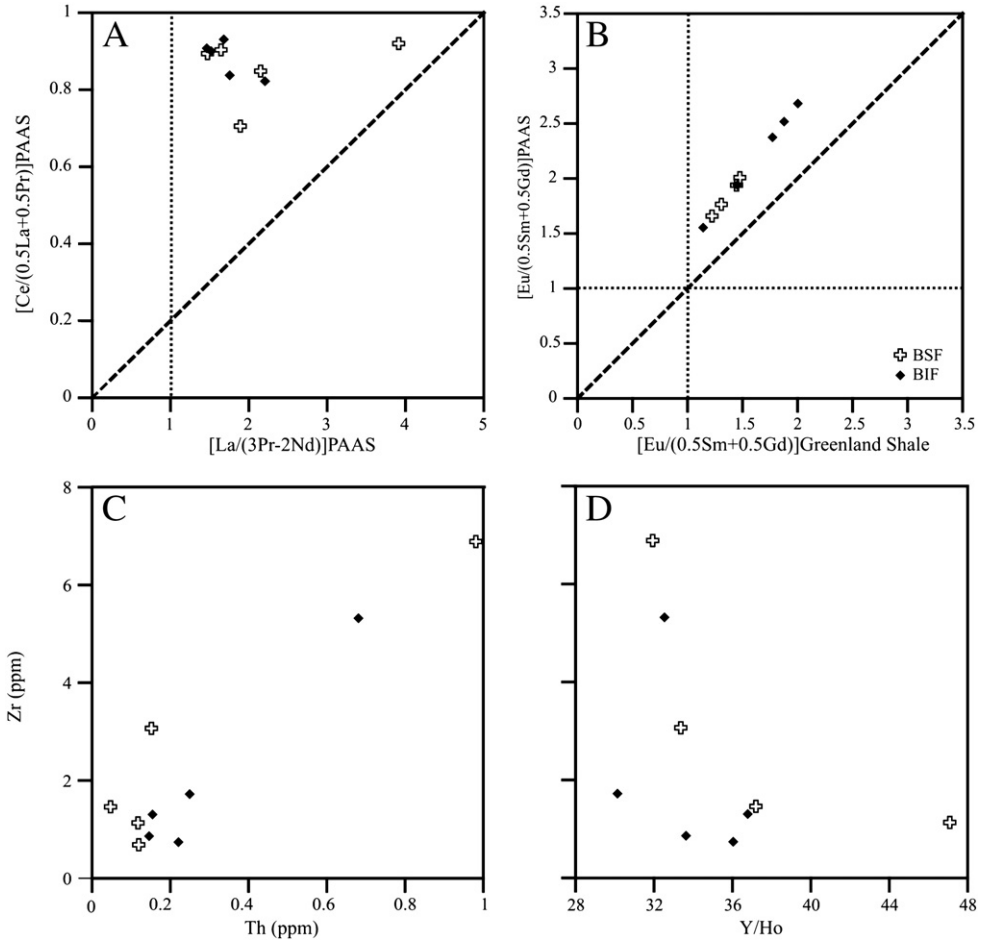

Fig. 7. (A) Positive La anomalies and negative Ce anomalies persist in all sample. (B) Eu anomalies persist in all BSF and BIF samples. Calculations for La, Eu and Ce anomaly verifications from Bolhar et al. (2004). (C) Plot comparing Zr over Th, and (D) plot comparing Zr over Y/Ho.

similar to that of modern-day seawater (Fig. 6B), with the exception of Eu and Ce anomalies (e.g. Bolhar et al., 2004). Sample 090710–12 has the highest REE + Y abundances of all the samples, and the flattest overall profile.

5. Discussion

5.1. Paragenesis

In order to infer the initial mineralogy of the Nuvvuagittuq BSF and BIF units, it is necessary to assess the metamorphic modifications that took place and establish the different stages of mineral genesis. The mineral assemblages in both units (i.e. magnetite, grunerite, actinolite, augite and quartz) are typical of an upper amphibolite/lower granulite facies assemblage for banded iron formation (e.g. Klein, 2005); these minerals are similarly well-represented in the quartz–magnetite BIFs of the Isua Supracrustal Belt (Dymek and Klein, 1988). Despite the multiphase metamorphic history of the Nuvvuagittuq belt (Cates and Mojzsis, 2009), petrographic evidence leads us to infer that the precursors of the BSF and BIF units consisted of ferric-oxyhydroxides, amorphous carbonate and silicate phases rich in Ca–Mg–Fe and amorphous silica. There was an insignificant clastic component.

Magnetite in BIF is generally thought to be a secondary product of diagenetic/metamorphic alteration of certain pre-existing Fe-rich mineral phases (Ayres, 1972). In the Nuvvuagittuq BSF and BIF, magnetite is the main Fe-oxide mineral present in either unit. It can commonly be found as inclusions within all the other mineral phase types suggesting that, of the current mineral phases, it was formed first. Magnetite can be the metamorphic by-product of hematite and siderite, at temperatures ranging from 480 °C to 650 °C and pressures of 5–12 kbar according to the following equation (Koziol, 2004):

$$3FeCO_{3(siderite)} + Fe_2O_{3(hematite)} \rightarrow Fe_3O_{4(magnetite)} + CO_2$$

The metamorphic grade of the Nuvvuagittuq belt would have been sufficient for this reaction to take place (Cates and Mojzsis, 2009). Ohmoto (2003) suggested that magnetite can also be formed through the reaction between pre-existing hematite and Fe(II)-rich hydrothermal fluids at <200 °C, resulting in the massive transformation of hematite to magnetite. However this scenario seems unlikely in this case, due to the lack of evidence for the supergene enrichment which would likely accompany such a flux of hydrothermal fluids. The production of biogenic magnetite *via* the reduction of ferric-oxyhydroxides through dissimilatory iron reduction (DIR; Lovley, 1993) is also an unlikely source for the magnetite in the Nuvvuagittuq chemical sediments. Whereas DIR typically produces magnetite with $\delta^{56}Fe < 0‰$ (Johnson et al., 2008), the heavy Fe isotope composition (up to 0.97‰ — Dauphas et al., 2007a; O'Neil et al., 2007) of these sediments led Dauphas et al. (2007a) to suggest that this signature was a product of the binary mixing between more primary Fe-oxides and carbonate deposits. It seems likely therefore, that the magnetite in these chemical sediments formed as a metamorphic by-product of hematite and siderite.

Quartz in iron formations is generally thought to be the stable end product of an initially amorphous silica precipitate that was recrystallized to chert and then to quartz at greenschist-facies conditions, as

denoted by the 120° triple junctions that characterize the granoblastic texture of the quartz (Klein, 2005; Trendall and Morris, 1983; Young, 1976). In the BSF and BIF units of the Nuvvuagittuq belt, quartz can be found as inclusions within grunerite and actinolite, while magnetite can be found as inclusions within the quartz, suggesting that the latter was the second phase, after magnetite, to crystallize.

Metamorphic Fe-bearing silicate minerals are commonly thought of as the products of metamorphic dehydration of pre-existing silicate and carbonate phases (Mel'nik, 1982). Grunerite can be produced in the reaction between quartz and siderite or the conversion from minnesotaite (Klein, 2005; Trendall and Morris, 1983):

$$8(Fe,Mg)CO_{3(siderite)} + 8SiO_{2(quartz)} + H_2O \rightarrow (Fe,Mg)_7Si_8O_{22}(OH)_{2(grunerite)} + 7CO_2$$

or

$$7Fe_2Si_4O_{10}(OH)_{2(minnesotaite)} \rightarrow 3Fe_7Si_8O_{22}(OH)_{2(grunerite)} + 4SiO_{2(quartz)} + 4SiO_2 + 4H_2O$$

The occurrence of actinolite as exsolution lamellae in grunerite is thought to be a result of selective crystallization from a homogeneous amphibole as a consequence of slow-cooling from amphibolite-facies peak metamorphic temperature (Ross et al., 1969). Clinopyroxene is a characteristic granulite-facies mineral, and occurs in BIF due to the decarbonation reaction between ankerite and quartz according to the following reaction (Klein, 2005):

$$Ca(Fe,Mg)(CO_3)_{2(ankerite)} + SiO_{2(quartz)} \rightarrow Ca(Fe,Mg)Si_2O_{6(clinopyroxene)} + 2CO_2$$

That augite as well as actinolite is present in Nuvvuagittuq chemical sediments suggests that some of the primary precipitates were Ca-bearing. Indeed, Dauphas et al. (2007a) concluded that in order to produce the range of Fe isotope compositions in the Nuvvuagittuq chemical sediments, binary mixing between Fe-oxides and some type of carbonate precursor was necessary. The precursors to the Fe-carbonates in most BIF are considered to have been very fine-grained carbonate oozes (Klein, 2005), however, the possibility that the source of Ca and Mg in the Nuvvuagittuq chemical sediments came from a Ca–Mg–Fe bearing silicate precursor cannot be ruled out.

5.2. Geochemistry

The composition of Archean chemical sediments ought to reflect input of solutes from both crustal weathering and hydrothermal emissions. Detrital input can also occur in shallow water facies iron formations, and such clastic particles tend to obscure the seawater signal.

Identification of a detrital component in BIF was done mainly through elevated concentrations of Al_2O_3, TiO_2 and high field strength elements — HFSE (e.g., Zr, Hf, Ta, Th) as well as through co-variations between HFSE and REE + Y ratios (La/La*, Y/Ho, Pr/Yb, Ce/Ce* — Bau, 1993; Bolhar et al. 2004; Ewers and Morris, 1981; McLennan et al., 1993). Despite being sandwiched in between high-Ti amphibolites below, and high-Al amphibolites above, both BIF and BSF units have low absolute concentrations of Al_2O_3 and TiO_2 concentrations (Al_2O_3: generally <0.5 wt.%; TiO_2: <0.03 wt.%). Concentrations of both REE + Y and HFSE are low in iron formations because dissolved REE + Y in the water column are normally scavenged by particulate matter before being adsorbed by Fe and Si gels on the seafloor, and input from a detrital source would commonly generate co-variations between HFSE and REE + Y in BIF (Bau, 1993). With the exception of samples 090710–13 (BSF) and 090710–12 (BIF), low concentrations of Zr, Hf, Ta and Th (<2.5 ppm) in the Nuvvuagittuq chemical sediments suggest little to no detrital input (Fig. 7C,D; Supplementary Data). The two aforementioned samples have slightly higher Zr, Hf, Ta and Th concentrations, low Y/Ho ratios and flatter REE + Y profiles (Fig. 6). However, even these concentrations are relatively low when compared to BIF with a recognized detrital component (e.g., Dales Gorge BIF).

The REE + Y profile of modern seawater is distinctive; the purest BIF and marine carbonates share certain seawater-like characteristics including (i) positive La and Eu anomalies; (ii) negative Ce anomalies (except for Archean BIFs); (iii) a relative depletion of LREE and MREE compared to HREE, and (iv) superchondritic Y/Ho ratios (i.e., >26) (Bau and Dulski, 1996; Bolhar et al., 2004). The reasons why these chemical sediments retain seawater-like REE + Y patterns are poorly understood, but the similarity of REE + Y profiles in BIF units spanning the Mesoarchean (Alexander et al., 2008) through the Proterozoic (e.g. Derry and Jacobsen, 1990 and references therein) demonstrates that they seem to reflect the seawater from which they precipitated. Apart from the negative Ce anomaly, all the aforementioned seawater-like anomalies are observed in the REE + Y profiles for both the Nuvvuagittuq BSF and BIF. In oxic seawater, soluble Ce(III) is converted to insoluble Ce(IV) and thus, the lack of Ce anomalies in Archean BIF has been used to infer prevailing anoxic conditions (e.g. Derry and Jacobsen, 1990; Kato et al., 1998). Although superchondritic Y/Ho ratios are a characteristic shared by both Archean BIF and modern ferromanganese crusts, shale-normalized Y anomalies are positive in the former and negative in the latter; it has been suggested that this could be related to the rate of deposition of ferric-oxyhydroxide particles (e.g., Bau and Dulski, 1996). The REE + Y in BIF are fairly immobile even at amphibolite facies metamorphism, and their mobility depends on high water/rock ratios (w/r>100) which are seldom achieved (Bau, 1991; Grauch, 1989). Of all the REE + Y, Eu is especially mobile due to the larger difference between its ionic radius and that of Fe^{2+}. Negative Eu anomalies, or inconsistent positive and negative Eu anomalies between samples, occur (Bau, 1993). The consistently positive Eu in all Nuvvuagittuq bulk samples suggests that there has been little REE + Y mobility.

It is possible to put a few constraints on the sources of REE + Y in the Nuvvuagittuq BSF and BIF. First, the strong positive Eu anomalies are distinctive of high-temperature (>350 °C) hydrothermal fluids. A conservative, two component mixing model between modern seawater and high-temperature hydrothermal fluids using Sm/Yb as a function of Eu/Sm implies that, like in the Isua BIF, a surprisingly small proportion of high-temperature hydrothermal fluids (<0.1%) were enough to cause such high Eu anomalies in the Nuvvuagittuq BSF and BIF (Fig. 8). Second, the Sm/Yb ratios of samples 0907010–13

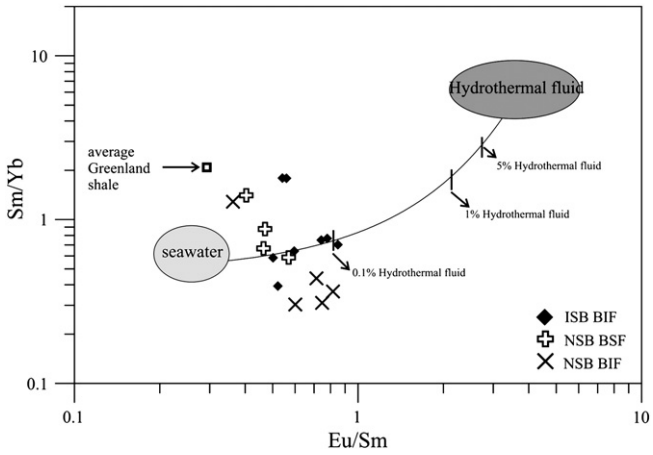

Fig. 8. Conservative, two-component mixing model of Sm/Yb vs. Eu/Sm ratios (after Alexander et al., 2008) for the Nuvvuagittuq BSF and BIF, Isua IF (Bolhar et al., 2004), high-temperature (>350 °C) hydrothermal fluids (Bau and Dulski, 1999), Pacific seawater (Alibo and Nozaki, 1999), and average Greenland shale (Bolhar et al., 2005).

(BSF), 090709–3 (BSF) and 090710–12 (BIF) are higher than the others and also display a subsequent decrease in Eu/Sm (Fig. 8), a signature which can be produced upon the addition of clastic material (e.g. Bau, 1993). No BIF is completely devoid of some detrital component, and although these samples also have the highest Zr, Hf, Ta, Th and REE + Y concentrations of all the samples, they still have seawater-like La/La* and Eu/Eu* anomalies, and no Ce/Ce* anomalies (Fig. 7A,B) which indicates that detrital inputs were minimal during chemical precipitation and the BSF and BIF units of the Nuvvuagittuq belt are relatively pure chemical sediments.

5.3. Comparing the Nuvvuagittuq chemical sediments with the Isua iron formations

Few Eoarchean-aged BIFs are known, and the recent discovery of the Nuvvuagittuq chemical sediments permits comparisons to be made with BIF from the Itsaq Gneiss Complex in West Greenland. Previous studies established that the chemical sediments from the Isua and Nuvvuagittuq belts have heavy δ^{56}Fe values (0.31–1.1 and 0.37–0.97‰, respectively), and these compositions are most parsimoniously explained through the partial oxidation of Fe via oxygenic or anoxygenic photosynthetic pathways (Dauphas et al., 2007a,b). These chemical sediments hold important implications for preserving not only the composition of Earth's earliest oceans, but also evidence of the earliest potential biosignatures.

From the perspective of mineralogy and metamorphic histories the amphibolite-facies Isua BIF and the upper-amphibolite/lower granulite facies Nuvvuagittuq chemical sediments show similarities in terms of relative trace element abundances, where Zn and Ni occur in the highest concentrations. Regarding absolute abundances however, Ni (Nuvvuagittuq median: 57 ppm; Isua median: 24 ppm) and Zn (Nuvvuagittuq median: 50 ppm; Isua median: 21 ppm) occur in slightly higher concentrations in the former (Appel, 1979; Bolhar et al. 2004; Dymek and Klein, 1988; Frei and Polat, 2007, Polat and Frei, 2005; Shimizu et al., 1990). Detrital indicators (Al_2O_3, TiO_2, HFSE) at both locations are low, which suggests that both locations are relatively detritus free. Their REE + Y profiles show seawater-like anomalies with a relative depletion in LREE compared to MREE and HREE, consistently positive La and Eu anomalies, negative Y/Ho ratios, and overall, similar REE + Y concentrations (e.g. Bolhar et al., 2004; Dymek and Klein, 1988). Moreover, ratios of Sm/Yb and Eu/Sm suggest that both the Isua and Nuvvuagittuq chemical sediments had similar contributions (~0.1%) by high-temperature hydrothermal sources (Fig. 8; Alexander et al., 2008). The similarities in the characteristics of the iron formations at Isua and Nuvvuagittuq would suggest that they were deposited under comparable environmental conditions, input sources and *via* the similar processes. This is the expected result for rocks of similar age and overall depositional setting.

5.4. Implications for the composition of the Eoarchean/Hadean oceans

It is widely held, though unsubstantiated due to the scarcity of an Eoarchean rock record, that metal requirements in microbes co-evolved with seawater metal availability through time (daSilva and Williams, 1991). As such, a key step in understanding the early evolution of life on Earth is to better understand the evolution of seawater composition. Studies that have sought to place quantitative constraints on the composition of the earliest oceans point to ferruginous waters (Holland, 1984) that were siliceous (Maliva et al., 2005), possibly mildly sulfidic (Saito et al., 2003), and likely contained an abundance of mafic–volcanic associated trace transition elements, such as Ni (Konhauser et al., 2009). Most BIFs older than ~2.0 Ga yr also possess chemical characteristics which suggest significant hydrothermal input into the oceans during their deposition, including positive Eu anomalies, a relative depletion of LREE in REE + Y profiles, and mantle-like Nd signatures (Beukes and Klein, 1990; Derry and Jacobsen, 1990; Jacobsen and Pimentel-Klose, 1988). Moreover, Isley (1995) estimated that, due to larger mantle heat flow during the Archean, rates of hydrothermal cycling were up to three times greater than at present, which provides an intimate link between the composition of solutes in seawater and the composition of oceanic crust, and by extension, mantle activity. Indeed, Isley and Abbott (1999) show a strong correlation between mantle plume activity and BIF occurrence through time.

With experimentally derived partitioning coefficients (K_D), it is possible to derive the concentration of a specific metal ion in the seawater from which chemical sediments precipitated. K_D values for Ni and Zn to ferric-oxyhydroxides were calculated in the laboratory using the methodology of Konhauser et al. (2007, 2009), and were then applied to bulk (i.e., XRF and ICP-MS) values of Ni, Zn and Fe in BIF; BSF rocks were not used as they contain sulfide grains that may imply secondary Zn enrichment (see Supplementary Data). Our calculations indicate that Ni values in the ocean at the time of the deposition of the Nuvvuagittuq BIF reached up to ~300 nM as compared to ~12 nM of modern seawater, while Zn concentrations appeared to have only reached up to ~20 nM as compared to ~9 nM in today's oceans (Bruland and Lohan, 2004).

It was recently proposed that the enhanced mantle partial-melting regime for peridotites in the Eo- and Mesoarchean and the related extrusion of Ni-rich ultra(mafic) volcanic rocks on the seafloor promoted high dissolved Ni concentrations in seawater; Archean-aged komatiite, tholeiites and basalts contained preferentially higher abundances of siderophile elements (e.g., Ni, Co, Cr, Fe) than their younger Proterozoic counterparts (e.g. Arndt, 1991; Taylor and McLennan, 1985) which could then become incorporated into BIF (Konhauser et al., 2009). Therefore, Ni-enrichment in the Nuvvuagittuq BIF is to be expected. Crucially, Ni is a key component in several enzymes of methane-producing bacteria (methanogens), and thus, its abundance would have facilitated increased methane production on the early Earth (Kida et al., 2001).

Zinc is also ultimately sourced from (ultra)mafic volcanics (Le Roux et al., 2010), and accordingly, one would predict high Zn concentrations in the Nuvvuagittuq BIF. However, translating Zn concentrations in BIF to seawater concentrations is complicated by the fact that a number of dissolved species and mineral phases have high sorptive capacities for Zn, and therefore Zn may not have accumulated in seawater. For instance, experimental data has shown that both ferric-oxyhydroxides and amorphous silica (Balistrieri et al., 2008; Pivovarov, 2008) can also sequester Zn, and thereby reduce its dissolved concentrations. In this regard, our application of K_D values for both Fe-only and silica-rich oceans both yield relatively low dissolved Zn concentrations. Planavsky et al. (2010) found that, based on the Zn composition of black shales through time, dissolved Zn concentrations in the Archean did not change significantly contrary to some suggestions (e.g., Dupont et al., 2010). Correspondingly, Zn concentrations in the Nuvvuagittuq BIF are comparable to Zn compositions in the Neoarchean (e.g., 2.75 Ga yr old Carájas Formation; Dymek and Klein, 1988), Paleoproterozoic (e.g., 2.3 Ga yr old Hotazel Formation BIF; Tsikos and Moore, 1997), and Neoproterozoic (590 Ma yr old Yerbal formation; Pecoits et al., in press).

Our results provide additional support for high Archean seawater Ni concentrations, and have important implications on Zn availability for early microbial metalloenzymes. Eukaryotes have a much more significant Zn requirement than prokaryotes, and previous studies have attributed the small number of ancient zinc enzymes (e.g., Dupont et al., 2006, 2010) to the non-bioavailability of Zn sulfide complexes, which dissociate slowly in seawater (Saito et al., 2003). Geochemical modeling results by Saito et al. (2003) suggest that even at dissolved sulfide levels on the order of 0.05 mM, enough sulfide exists in solution, following the formation of $FeHS^+$, to completely complex trace metals such as Cu, Cd and Zn. However, results from

Table 2
Model output results examining the effect of sulfide and increasing iron on Zn and Ni speciation in Archean seawater. Models are for speciation, and do not assume precipitation.

Component	Species name	0.05 mM Fe^{2+}	1.8 mM Fe^{2+}
		%total concentration	%total concentration
Sulfide	HS^{-1}	47.632	0.525
	$H_2S_{(aq)}$	10.227	0.113
	$FeHS^{+}$	42.09	99.346
Zinc	Zn^{+2}	7.402	59.658
	$ZnOH^{+}$	0.094	0.757
	$Zn(OH)_{2(aq)}$	0.024	0.197
	$ZnCl^{+}$	2.509	20.24
	$ZnCl_4^{-2}$	0.089	0.718
	$ZnCl^{3-}$	0.24	1.934
	$ZnCl_{2(aq)}$	0.469	3.784
	$Zn_2S_3^{-2}$	9.779	
	$ZnS_{(aq)}$	78.683	6.998
	$ZnCO_{3(aq)}$	0.451	3.623
	$ZnHCO^{3+}$	0.258	2.072
	$Zn(CO_3)_2^{-2}$		0.02
Nickel	Ni^{+2}	18.074	78.874
	$NiOH^{+}$	0.029	0.126
	NiCl +	0.789	3.447
	$NiCl_{2(aq)}$		0.023
	$NiHS^{+}$	77.935	3.755
	$NiCO_{3(aq)}$	0.711	3.092
	$NiHCO^{3+}$	2.456	10.681

geochemical modeling experiments generated using Visual MINTEQ 3.0 (Gustafsson, 2011 — at 1 mM HS; 10 mM each of Ni and Zn alongside other trace metals; 50 μM Fe^{2+}, a conservative estimate after Holland, 1984; and under similar experimental parameters as in Saito et al., 2003), alternatively suggest that ~0.7 nM of Zn^{2+} and ~1.8 nM of Ni^{2+} would remain as free ions. When Fe is increased towards an upper limit for the Archean oceans (1.8 mM, Edmond et al., 1982), these values increase to ~6 and 7.9 nM for Zn^{2+} and Ni^{2+} respectively, that remain uncomplexed by sulfides (Table 2; see Supplementary Data for full modeling results and parameters). Although some of the Zn present in the Nuvvuagittuq BIFs likely sorbed onto ferric-oxyhydroxide particles in the form of Zn sulfide complexes, our findings suggest that a biologically significant fraction of Zn and Ni is likely to have been in a bioavailable form (e.g., chloro-, hydroxyl-, or uncomplexed). This is similar to previous findings suggesting the utilization, and thereby bioavailable nature, of Ni in the metalloenzymes of methanogens (Kida et al., 2001; Konhauser et al., 2009).

6. Conclusions

Petrographic and geochemical analyses of chemical sediments in the Nuvvuagittuq Supracrustal Belt in northern Québec (Canada) lead us to conclude that:

1. There are two distinct chemical sedimentary units in the Nuvvuagittuq belt, a BIF unit consisting of alternating microbands of magnetite, Fe–Mg–Ca silicates and quartz, and a more silicate rich unit consisting of alternating microbands of quartz and Fe–Mg–Ca silicates (BSF).
2. The primary precipitates to these units were Fe–Mg–Ca-bearing silicate and/or carbonate minerals, chert, siderite and hematite. The precursor deposits were made up of layered amorphous silica and ferric-oxyhydroxides, fine grained carbonate oozes and/or Fe–Mg–Ca rich silicate gels.
3. Low Al_2O_3, TiO_2, Zr, Hf, Ta and Th concentrations in most of the BSF and BIF samples suggest detritus-free chemical sediments; REE + Y profiles with distinctive seawater-like signatures. Furthermore, consistently positive Eu anomalies suggest that these units have preserved much of their seawater-like composition despite metamorphic overprinting, with an ~0.1% contribution by high-temperature hydrothermal fluids, similar to the Isua BIF.
4. The most significant trace elements in the Nuvvuagittuq chemical sediments are Ni and Zn, with relative depletions (<15 ppm) in all other trace elements. In the BSF, Ni and Zn are particularly abundant in grunerite and actinolite. In the BIF, Ni is particularly abundant in magnetite, while Zn is abundant in grunerite and actinolite. The application of experimentally-derived partitioning coefficients to absolute concentrations in the BIF show that, compared to modern seawater, Earth's earliest oceans had relatively high dissolved Ni concentrations (up to ~300 nM), but somewhat similar Zn concentrations (up to ~20 nM). A biologically significant portion of the zinc was likely to have occurred as Zn^{2+} and able to form bioavailable complexes.
5. The petrographic and compositional similarities between the chemical sediments in the Nuvvuagittuq and Isua Supracrustal Belts suggest very similar depositional environments in terms of seawater composition, as well as relative input sources.

Acknowledgments

We wish to thank Dr. Sergei Matveev and Guangcheng Chen for their assistance in the microprobe and LA-ICP-MS analyses, respectively. We especially thank Dr. Don Francis for facilitating the organization of field logistics, and Dr. Emilie Thomassot, Dr. Médéric Palot and Yumi Kitayama for their assistance in the field. We would also like to thank the community of Inukjuak and the Pituvik Landholding Corporation, especially Mike Carroll, Johnny Mina, Minnie Palliser, Simeonie Elyasiapik and Aliva Epoo. For their invaluable help in camp, we thank Minnie Nowkawalk and Noah Echalook. This work was supported by a National Sciences and Engineering Research Council of Canada award to KOK. NLC and SJM acknowledge support from the NASA Exobiology and Evolutionary Biology Program. Additional support to SJM came from NASA Lunar Science Institute, National Geographic Society, University of Colorado Office of the President, and the J. William Fulbright Foundation.

Appendix A. Supplementary data

Supplementary data to this article can be found online at doi:10.1016/j.epsl.2011.11.020.

References

Alexander, B.W., Bau, M., Andersson, P., Dulski, P., 2008. Continentally-derived solutes in shallow Archean seawater: rare earth element and Nd isotope evidence in iron formation from the 2.9 Ga Pongola Supergroup, South Africa. Geochim. Cosmochim. Acta 72, 378–394.
Alibo, D.S., Nozaki, Y., 1999. Rare earth elements in seawater: particle association, shale-normalization, and Ce oxidation. Geochim. Cosmochim. Acta 63, 363–372.
Appel, P.W.U., 1979. Cosmic grains in an iron-formation from the Early Precambrian Isua Supracrustal Belt, West Greenland. J. Geol. 87, 573–578.
Arndt, N.T., 1991. High Ni in Archean tholeiites. Tectonophysics 187, 411–419.
Ayres, D.E., 1972. Genesis of iron-bearing minerals in banded iron formation mesobands in The Dales Gorge Member, Hamersley Group, Western Australia. Econ. Geol. 67, 1214–1233.
Balistrieri, L.S., Borrok, D.M., Wanty, R.B., Ridley, W.I., 2008. Fractionation of Cu and Zn isotopes during adsorption onto amorphous Fe(III) oxyhydroxide: experimental mixing of acid rock drainage and ambient river water. Geochim. Cosmochim. Acta 72, 311–328.
Bau, M., 1991. Rare-earth element mobility during hydrothermal and metamorphic fluid-rock interaction and the significance of the oxidation state of europium. Chem. Geol. 93, 219–230.
Bau, M., 1993. Effects of syn- and post-depositional processes on the rare-earth element distribution in Precambrian iron-formations. Eur. J. Mineral. 5, 257–267.
Bau, M., Dulski, P., 1996. Distribution of yttrium and rare-earth elements in the Penge and Kuruman iron-formations, Transvaal Supergroup, South Africa. Precambrian Res. 79, 37–55.
Bau, M., Dulski, P., 1999. Comparing yttrium and rare earths in hydrothermal fluids from the Mid-Atlantic Ridge: implications for Y and REE behaviour during near-vent mixing and for the Y/Ho ratio of Proterozoic seawater. Chem. Geol. 155, 77–90.

Beukes, N.J., Klein, C., 1990. Geochemistry and sedimentology of a facies transition – from microbanded to granular iron-formation – in the early Proterozoic Transvaal Supergroup, South Africa. Precambrian Res. 47, 99–139.
Bjerrum, C.J., Canfield, D.E., 2002. Ocean productivity before about 1.9 Gyr ago limited by phosphorus adsorption onto iron oxides. Nature 417, 159–162.
Boily, M., Leclair, A., Maurice, C., Bédard, J.H., David, J., 2009. Paleo- to Mesoarchean basement recycling and terrane definition in the Northeastern Superior Province, Québec, Canada. Precambrian Res. 168, 23–44.
Bolhar, R., Kamber, B.S., Moorbath, S., Fedo, C.M., Whitehouse, M.J., 2004. Characterisation of early Archaean chemical sediments by trace element signatures. Earth Planet. Sci. Lett. 222, 43–60.
Bolhar, R., Van Kranendonk, M.J., Kamber, B.S., 2005. A trace element study of siderite–jasper banded iron formation in the 3.45 Ga Warrawoona Group, Pilbara Craton—formation from hydrothermal fluids and shallow seawater. Precambrian Res. 137, 93–114.
Bruland, K.W., Lohan, M.C., 2004. The control of trace metals in seawater. In: Elderfield, H. (Ed.), The Oceans and Marine Geochemistry: The Treatise of Geochemistry, pp. 33–47.
Cates, N.L., Mojzsis, S.J., 2006. Chemical and isotopic evidence for widespread Eoarchean metasedimentary enclaves in southern West Greenland. Geochim. Cosmochim. Acta 70, 4229–4257.
Cates, N.L., Mojzsis, S.J., 2007. Pre-3750 Ma supracrustal rocks from the Nuvvuagittuq supracrustal belt, northern Québec. Earth Planet. Sci. Lett. 255, 9–21.
Cates, N.L., Mojzsis, S.J., 2009. Metamorphic zircon, trace elements and Neoarchean metamorphism in the ca. 3.75 Ga Nuvvuagittuq supracrustal belt, Québec (Canada). Chem. Geol. 261, 99–114.
daSilva, J.J.R.F., Williams, R.J.P., 1991. The Biological Chemistry of the Elements: The Inorganic Chemistry of Life, 2nd ed. Oxford University Press, Oxford.
Dauphas, N., van Zuilen, M., Wadhwa, M., Davis, A.M., Marty, B., Janney, P.E., 2004. Clues from Fe isotope variations on the origin of Early Archean BIFs from Greenland. Science 306, 2077–2080.
Dauphas, N., Cates, N.L., Mojzsis, S.J., Busigny, V., 2007a. Identification of chemical sedimentary protoliths using iron isotopes in the >3750 Ma Nuvvuagittuq supracrustal belt, Canada. Earth Planet. Sci. Lett. 254, 358–376.
Dauphas, N., van Zuilen, M., Busigny, V., Lepland, A., Wadhwa, M., Janney, P.E., 2007b. Iron isotope, major and trace element characterization of early Archean supracrustal rocks from SW Greenland: protolith identification and metamorphic overprint. Geochim. Cosmochim. Acta 71, 4745–4770.
David, J., Godin, L., Stevenson, R., O'Neil, J., Francis, D., 2009. U–Pb ages (3.8–2.7 Ga) and Nd isotope data from the newly identified Eoarchean Nuvvuagittuq supracrustal belt, Superior Craton, Canada. Geol. Soc. Am. Bull. 121, 150–163.
Deer, W.A., Howie, R.A., Zussman, J., 1992. An Introduction to the Rock Forming Minerals. Prentice Hall.
Derry, L.A., Jacobsen, S.B., 1990. The chemical evolution of Precambrian seawater: evidence from REEs in banded iron formations. Geochim. Cosmochim. Acta 54, 2965–2977.
Dupont, C.L., Yang, S., Palenik, B., Bourne, P.E., 2006. Modern proteomes contain putative imprints of ancient shifts in trace metal geochemistry. Proc. Natl. Acad. Sci. 103, 17822–17827.
Dupont, C.L., Butcher, A., Valas, R.E., Bourne, P.E., Caetano-Anollés, G., 2010. History of biological metal utilization inferred through phylogenomic analysis of protein structures. Proc. Natl. Acad. Sci. 107, 10567–10572.
Dymek, R.F., Klein, C., 1988. Chemistry, petrology and origin of banded iron-formation lithologies from the 3800 Ma Isua supracrustal belt, West Greenland. Precambrian Res. 39, 247–302.
Edmond, J.M., Von Damm, K.L., McDuff, R.E., Measures, C.I., 1982. Chemistry of hot springs on the East Pacific Rise and their effluent dispersal. Nature 297, 187–191.
Ewers, W.E., Morris, R.C., 1981. Studies of the Dales Gorge Member of the Brockman Iron Formation, Western Australia. Econ. Geol. 76, 1929–1953.
Frei, R., Polat, A., 2007. Source heterogeneity for the major components of 3.7 Ga banded iron formations (Isua Greenstone Belt, Western Greenland): tracing the nature of interacting water masses in BIF formation. Earth Planet. Sci. Lett. 253, 266–281.
Grauch, R.I., 1989. Rare earth elements in metamorphic rocks. Rev. Mineral. Geochem. 21, 147–167.
Gustafsson, J.P., 2011. Visual Minteq, 3.0 ed. http://www.lwr.kth.se/English/OurSoftware/vminteq (Stockholm, Sweden).
Hamade, T., Konhauser, K.O., Raiswell, R., Morris, R.C., Goldsmith, S., 2003. Using Ge:Si ratios to decouple iron and silica fluxes in Precambrian banded iron formations. Geology 31, 35–38.
Holland, H.D., 1984. The Chemical Evolution of the Atmosphere and Oceans. Princeton University Press, Princeton, NJ.
Isley, A.E., 1995. Hydrothermal plumes and the delivery of iron to banded iron formation. J. Geol. 103, 169–185.
Isley, A.E., Abbott, D.H., 1999. Plume-related mafic volcanism and the deposition of banded iron formation. J. Geophys. Res. 104, 15461–15477.
Jacobsen, S.B., Pimentel-Klose, M.R., 1988. A Nd isotopic study of the Hamersley and Michipicoten banded iron formations: the source of REE and Fe in Archean oceans. Earth Planet. Sci. Lett. 87, 29–44.
Johnson, C.M., Beard, B.L., Klein, C., Beukes, N.J., Roden, E.E., 2008. Iron isotopes constrain biologic and abiologic processes in banded iron formation genesis. Geochim. Cosmochim. Acta 72, 151–169.
Kato, Y., Ohta, I., Tsunematsu, T., Watanabe, Y., Isozaki, Y., Maruyama, S., Imai, N., 1998. Rare earth element variations in mid-Archean banded iron formations: implications for the chemistry of ocean and continent and plate tectonics. Geochim. Cosmochim. Acta 62, 3475–3497.
Kida, K., Shigematsu, T., Kijima, J., Numaguchi, M., Mochinaga, Y., Abe, N., Morimura, S., 2001. Influence of Ni^{2+} and Co^{2+} on methanogenic activity and the amounts of coenzymes involved in methanogenesis. J. Biosci. Bioeng. 91, 590–595.
Klein, C., 2005. Some Precambrian banded iron-formations (BIFs) from around the world: their age, geologic setting, mineralogy, metamorphism, geochemistry, and origins. Am. Mineral. 90, 1473–1499.
Konhauser, K.O., Hamade, T., Raiswell, R., Morris, R.C., Ferris, F.G., Southam, G., Canfield, D.E., 2002. Could bacteria have formed the Precambrian banded iron formations? Geology. 30, 1079–1082.
Konhauser, K.O., Lalonde, S.V., Amskold, L., Holland, H.D., 2007. Was there really an Archean phosphate crisis? Science 315, 1234.
Konhauser, K.O., Pecoits, E., Lalonde, S.V., Papineau, D., Nisbet, E.G., Barley, M.E., Arndt, N.T., Zahnle, K., Kamber, B.S., 2009. Oceanic nickel depletion and a methanogen famine before the Great Oxidation Event. Nature 458, 750–753.
Koziol, A.M., 2004. Experimental determination of siderite stability and application to Martian Meteorite ALH84001. Am. Mineral. 89, 294–300.
Le Roux, V., Lee, C.T.A., Turner, S.J., 2010. Zn/Fe systematics in mafic and ultramafic systems: implications for detecting major element heterogeneities in the Earth's mantle. Geochim. Cosmochim. Acta 74, 2779–2796.
Lovley, D.R., 1993. Dissimilatory metal reduction. Annu. Rev. Microbiol. 47, 263–290.
Maliva, R.G., Knoll, A.H., Simonson, B.M., 2005. Secular change in the Precambrian silica cycle: insights from chert petrology. Geol. Soc. Am. Bull. 117, 835–845.
Manning, C.E., Mojzsis, S.J., Harrison, T.M., 2006. Geology, age and origin of supracrustal rocks at Akilia, West Greenland. Am. J. Sci. 306, 303–366.
McLennan, S.M., Hemming, S., McDaniel, D.K., Hanson, G.N., 1993. Geochemical approaches to sedimentation, provenance, and tectonics. Special Papers — Geological Society of America, pp. 21–40.
Mel'nik, Y.P., 1982. Precambrian Iron Formations: Physiochemical Conditions of Formation. Elsevier Scientific Publishing Company.
Nutman, A.P., McGregor, V.R., Friend, C.R.L., Bennett, V.C., Kinny, P.D., 1996. The Itsaq Gneiss Complex of southern West Greenland; the world's most extensive record of early crustal evolution (3900–3600 Ma). Precambrian Res. 78, 1–39.
Ohmoto, H., 2003. Nonredox transformations of magnetite–hematite in hydrothermal systems. Econ. Geol. 98, 157–161.
O'Neil, J., Maurice, C., Stevenson, R.K., Larocque, J., Cloquet, C., David, J., Francis, D., 2007. The Geology of the 3.8 Ga Nuvvuagittuq (Porpoise Cove) Greenstone Belt, Northeaster Superior Province, Canada. Developments in Precambrian Geology 15, 219–250.
O'Neil, J., Carlson, R.W., Francis, D., Stevenson, R.K., 2008. Neodymium-142 evidence for Hadean Mafic Crust. Science 321, 1828–1831.
O'Neil, J., Francis, D., Carlson, R., 2011. Implications of the Nuvvuagittuq Greenstone Belt for the formation of Earth's early crust. J. Petrol. 52, 985–1009.
Pecoits, E., Aubet, N.R., Gingras, M.K., Poulton, S.W., Bekker, A., Veroslavsky, G., Konhauser, K.O., in press. An Ediacaran iron formation: New evidence for ferruginous late Neoproterozoic seawater. Precambrian Research.
Pivovarov, S., 2008. Adsorption of ions onto amorphous silica: ion exchange model. J. Colloid Interface Sci. 319, 374–376.
Planavsky, N.J., Scott, C., Bekker, A., Lyons, T.W., 2010. Tracking Zn bioavailability through time: new insights from sulfidic black shales. American Geophysical Union, Fall Meeting, 2010, Abstract #OS33E-1510. .
Polat, A., Frei, R., 2005. The origin of early Archean banded iron formations and of continental crust, Isua, southern West Greenland. Precambrian Res. 138, 151–175.
Ross, M., Papike, J.J., Shaw, K.W., 1969. Exsolution textures in amphiboles as indicators of subsolidus thermal histories. Mineralog. Soc. Amberica Spec. Pap. 2, 275–299.
Saito, M.A., Sigman, D.M., Morel, F.M.M., 2003. The bioinorganic chemistry of the ancient ocean: the co-evolution of cyanobacterial metal requirements and biogeochemical cycles at the Archean–Proterozoic boundary? Inorg. Chim. Acta 356, 308–318.
Shimizu, H., Umemoto, N., Masuda, A., Appel, P.W.U., 1990. Sources of iron-formations in the Archean Isua and Malene supracrustals, West Greenland: evidence from La–Ce and Sm–Nd isotopic data and REE abundances. Geochim. Cosmochim. Acta 54, 1147–1154.
Stevenson, R.K., David, J., Parent, M., 2006. Crustal evolution of the western Minto Block, northern Superior Province, Canada. Precambrian Res. 145, 229–242.
Taylor, S.R., McLennan, S.M., 1985. The Continental Crust: Its Composition and Evolution.
Trendall, A.F., Morris, R.C., 1983. Iron Formations: Facts and Problems. Elsevier Scientific Publishers Inc.
Tsikos, H., Moore, J.M., 1997. Petrography and geochemistry of the Paleoproterozoic Hotazel Iron-Formation, Kalahari manganese field, South Africa; implications for Precambrian manganese metallogenesis. Econ. Geol. 92, 87–97.
Whitehouse, M.J., Fedo, C.M., 2007. Microscale heterogeneity of Fe isotopes in >3.71 Ga banded iron formation from the Isua Greenstone Belt, southwest Greenland. Geology 35, 719–722.
Young, S.W., 1976. Petrographic textures of detrital polycrystalline quartz as an aid to interpreting crystalline source rocks. J. Sed. Res. 46, 595–603.